Mycolates of Mycobacterium tuberculosis modulate the flow of cholesterol for bacillary proliferation in murine macrophages

Vermeulen, Ilke; Baird, Mark; Al-Dulayymi, Juma'a; Smet, Muriel; Verschoor, Jan; Grooten, Johan

Journal of Lipid Research

DOI:
10.1194/jlr.M073171

Published: 01/04/2017

Peer reviewed version

Mycolates of *Mycobacterium tuberculosis* modulate the flow of cholesterol for bacillary proliferation in murine macrophages

Ilke Vermeulen[1,2], Mark Baird[3], Juma Al-Dulayymi[3], Muriel Smet[1], Jan Verschoor[2], and Johan Grooten[1]

[1]Laboratory of Molecular Immunology, Department of Biomedical Molecular Biology, Ghent University, Technologiepark 927, Ghent Zwijnaarde 9052, Belgium

[2]Department of Biochemistry, University of Pretoria, Pretoria 0002, South Africa

[3]School of Chemistry, Bangor University, Bangor, Gwynedd, Wales, LL57 2UW, UK

Running title: *Mtb mycolates intercept cholesterol for mycobacterial growth*

Corresponding author: Johan Grooten, Department of Biomedical Molecular Biology, Ghent University, Belgium; Telephone: (0032) 9-331-3689; Fax: (0032) 9-221-7673; E-mail: Johan.Grooten@irc.ugent.be.

Footnotes (abbreviations used): αMA, alpha-MA; BCG, *M. bovis* bacille Calmette-Guérin; GLM, generalised linear model; kMA, keto-MA; LD, lipid droplet; LXR, liver X receptor; MA, mycolic acid; mMA, methoxy-MA; MGC, multinucleated giant cell; Mtb, *Mycobacterium tuberculosis*; TB, tuberculosis.

Abstract

The differentiation of macrophages into lipid-filled foam cells is a hallmark of the lung granuloma that forms in patients with active tuberculosis (TB). Mycolic acids (MAs), the abundant lipid virulence factors in the cell wall of *Mycobacterium tuberculosis* (Mtb), can induce this foam phenotype possibly as a way to perturb host cell lipid homeostasis to support the infection. It is not exactly clear how MAs allow differentiation of foam cells during Mtb infection. Here we investigated how chemically synthetic MAs, each with a defined stereochemistry similar to natural Mtb-associated mycolates, influence cell foamy phenotype and mycobacterial proliferation in murine host macrophages. Using light and laser-scanning-confocal microscopy, we assessed the influence of MA structure first on the induction of granuloma cell types, second on intracellular cholesterol accumulation, and finally on mycobacterial growth. While methoxy mycolates (mMA) effected multi-vacuolar giant cell formation, keto-MAs (kMA) induced abundant intracellular lipid droplets (LDs) that were packed with esterified cholesterol. Macrophages from mice treated with kMA were permissive to mycobacterial growth, whereas cells from mMA treatment were not. This suggests a separate yet key involvement of oxygenated MAs in manipulating host cell lipid homeostasis to establish the state of TB.

Keywords: cholesterol, confocal microscopy, foam cell, infection, lipid droplets, liver X receptor, macrophages, *Mycobacterium tuberculosis*, mycolic acid, tuberculosis

Introduction

Mycobacterium tuberculosis (Mtb), the aetiological agent of tuberculosis (TB), infects approximately 2-3 billion people globally (1). Though only a minority of infected individuals (<15%) will develop pulmonary disease during their lifetime, most remain prolonged asymptomatic carriers that may develop active disease later on (1). In this instance bacilli are not entirely cleared, but remain in a state of dormancy inside its host. Throughout this period, Mtb resides inside lung granulomas, the main histopathology of TB (2). The granuloma milieu is characterised by a multifaceted host immune response of containment and destruction, yet Mtb bacilli are able to counteract and evade host defences (3-5). During active TB, granulomas are characterised by large cell aggregates of lymphocytes, neutrophils, dendritic cells and peripheral fibroblasts (6). Key effector cells of granuloma formation are macrophages, which can differentiate into vacuolar multinucleated giant cells (MGCs) or lipid-laden foam cells (7). Tuberculous bacilli may reside in foam cells or escape into the cell-free caseous centre of the granuloma (2, 7). The biochemical signalling pathways involved in foamy phenotype regulation remain understudied. Growing evidence indicates that an advanced metabolic network stands at the centre of the unique adaptation of Mtb in its host macrophage (8-10), regulating the manifestation of latent, chronic or acute TB.

The Mtb cell envelope comprises intricate layers of peptidoglycan, arabinogalactan, glycolipids, mycolic acids (MAs; α-alkyl, β-hydroxy fatty acids) and lipoproteins, with MAs being the dominant constituent (11, 12). The structural and biochemical properties of MAs have been reviewed recently (13). In short, these wax-like hydrophobic lipids comprise a mycolic motif with long non-functionalised alkyl chain and a meromycolate chain with up to two functional groups that can be either oxygenated (distal group) or unoxygenated (distal or proximal group) (13). Three main Mtb MA classes exist: the most abundant unoxygenated alpha-MA (αMA), the less abundant oxygenated methoxy- (mMA) and the least abundant keto-MA (kMA; Fig. 1) (14, 15). Orientation of the proximal cyclopropane differs. αMA essentially exists in *cis*- configuration (though a small amount of *trans*- may be present), whereas mMA and kMA

contain either *cis*- or *trans*-cyclopropanation with an adjoining methyl branch (11). Whilst the level of αMA is fixed at ~53% and oxygenated MA at ~47%, the ratio between the two oxygenated MAs varies with methoxy at 32-40% and keto at 7-15% (16), depending on the growth stage of the bacilli (17-19). Mtb envelope derived lipids potently influence host immunity (20-22), while host cell lipidomes are exploited by intracellular pathogens like Mtb to gain entry and replicate (23). The work by Cole *et al.* on deciphering the Mtb genome identified two distinct sets of complex enzymatic machinery for successive biosynthesis of fatty acids, meromycolates and long carbon chain MAs (24). A MA-rich cell wall that can be altered depending on physiological requirements is essential for Mtb virulence (17, 18). We previously showed that *in vivo* MA treatment induced peritoneal and alveolar macrophages of the foam phenotype in mice (25, 26), similar to that in macrophages from the TB granuloma (27). At the onset of TB infection, foam cells form that are characteristically enlarged and filled with multiple lipid droplets (LD) and vacuoles (28, 29). Cholesterol is abundantly distributed across cell membranes and forms a major constituent of LDs (30, 31). It also plays a unique role in Mtb virulence and pathogenesis. Mtb preferentially catabolises cholesterol as nutrient source whilst its acquisition, through a unique Mtb import system, is necessary to establish and maintain persistent infection (32, 33). In macrophages, the genetic regulator of cellular cholesterol homeostasis is the liver X receptor (LXR) (34). LXRs are transcription factors that act as cholesterol sensors and that maintain the balance of cholesterol uptake and export through regulation of expression of cholesterol-associated target genes (35).

To better understand the mechanisms responsible for the establishment of active TB related granulomas, we investigated how *in vivo* treatment of mice with chemically synthetic MAs, each with a defined stereochemistry representing the separate major classes of Mtb mycolates, influence cell differentiation and support of mycobacteria in peritoneal macrophages. We assessed the influence of MA structure first on the induction of foamy macrophages and MGCs identified by light and laser-scanning-confocal microscopy, second on cholesterol accumulation and finally on intracellular mycobacterial growth. Our results show that Mtb mycolates differentially steer host macrophages to either an enlarged vacuolar or a

lipid-laden foamy phenotype. We report it is kMA that induced mainly cholesterol ester accumulation and intracellular LDs to sustain facilitation of mycobacterial BCG proliferation. mMA was found to induce vacuolation with no change in cholesterol ester levels, nor improved ability to sustain and facilitate mycobacterial growth. αMA treatment had a negligible effect on these parameters. To determine how foam cells brought about by non-tuberculous means compares to foam cells induced by the different mycolates, we also investigated cholesterol accumulation and mycobacterial growth of peritoneal macrophages from LXR-deficient mice. In macrophages with a deficiency in LXR activity that is characterised by perturbed cholesterol transport or export, we recorded foam cells with abundant cholesterol ester containing LDs that showed elevated BCG replication.

Materials and methods

Mycolic acids

Natural MA mixture was isolated and single synthetic MAs synthesised as previously described (16, 36-38). The single MAs used for *in vivo* murine treatment in this study all contained *cis*-cyclopropanation, referring to the orientation of the proximal cyclopropane. MA treatments comprised *cis*-αMA, *cis*-mMA, *cis*-kMA consisting of a mixture of both epimers of the distal α-methyl-ketone group with S- and R-stereochemistry, and a natural isolated mixture of all three MA classes (each as a complex mixture of homologues) similar to the natural composition of MAs in the Mtb cell wall (MA mix) (Fig. 1), i.e. ~53% αMA, ~38% mMA and ~9% kMA.

Animals

Mice used were specific pathogen-free C57BL/6 WT females, aged eight to twelve weeks (Janvier Labs, France). C57BL/6Bom WT and LXR$\alpha^{-/-}\beta^{-/-}$ mice (39) were bred in the animal facility of Ghent University. Animals were housed individually in a temperature- and light- controlled facility and received mixed ration feed and water *ad libitum*. Experiments were preapproved by the Ghent University Ethical

Committee for Animal Experimentation in accordance with current European laws regarding the welfare and humane use of animals.

Experimental design

Mice were treated intraperitoneally (i.p.) with various control or MA solutions two days prior to harvesting of peritoneal exudate cells (PEC). Macrophages from PEC were cultured for three days and live cells fluorescently labelled for foam cell markers and examined by laser-scanning-confocal microscopy on each day (0 h, 24 h and 48 h time points). The mycobacterial model was similar to the foam cell model except that following overnight adherence, cells were infected for 6 h with *M. bovis* bacille Calmette-Guérin expressing the dsRed fluorescent protein (BCG-dsRed; a gift from Prof. Ben Appelmelk from the Department of Medical Microbiology and Infection Control at the VU University Medical Centre in Amsterdam via the Unit of Medical Biotechnology at the Inflammation Research Center in Ghent). After three washes with endotoxin-free PBS (Lonza), the cells were stained with fluorescent markers for confocal microscopy (0 h) to assess macrophage morphotype or left for up to five days to measure mycobacterial growth (48 h and 96 h). The LXR model was similar to the mycobacterial model apart from mice were not treated with MAs prior to harvesting PEC.

Mycobacterial culture and infection

BCG-dsRed has been described previously (40). The BCG strain Copenhagen (Danish 1331) was used here (41), which has no mMA, but similar quantities each of αMA and kMA (42). Bacterial cultures were grown in Middlebrook 7H9 broth (Difco) supplemented with 0.2% glycerol, 0.05% Tween-80 and 10% Middlebrook AODC enrichment containing oleic acid, albumin, dextrose and catalase (Becton Dickinson). BCG expanded to an OD_{600nm} of 0.8-1.0 was used to infect cells *ex vivo* at a multiplicity of infection (MOI) of 1 bacterium per cell for 6 h. Following the 6 h infection, cells were washed three times with warm endotoxin-free PBS and cultured at 37°C and 5% CO_2.

Injectable solutions and macrophage isolation

Liposomes were used as carrier to deliver the highly hydrophobic MA compounds to target cells. As a first step, L-α-Phosphatidylcholine (PC, Sigma®) powder was dissolved in chloroform at 100 mg/ml (10% w/v). PC and MA dissolved in chloroform were vortexed and heated before undergoing dehydration on a heat block (90°C) and the dried lipids recovered in endotoxin-free PBS. Solutions underwent a series of vortex and sonication steps at 65°C until homogenous milky consistency. Mice were immediately treated *in vivo* by i.p. injection (25 µg MA/100 µl/mouse). A liposome control (Lipo) was formulated as described for the MA solutions, but without the addition of any synthetic MA. Two days after *in vivo* treatment, mice were euthanized via cervical dislocation and PECs harvested by peritoneal lavage. Mouse abdomens were decontaminated with 70% ethanol and 10 ml ice cold endotoxin-free PBS injected i.p. Following a short abdominal massage, PECs were removed into sterile 15 ml tubes and kept on ice until further processing by centrifugation (1200 rpm, 4°C, 10 min) and red blood cell lysis (ACK lysing buffer, Lonza; 50% v/v). PECs were seeded in 250 µl culture medium ($5x10^5$ cells) in µ-Slide 8-well microscopy plates (Ibidi®). Culture medium consisted of RPMI 1640 (Gibco®) supplemented with LPS-free and heat-inactivated FCS (10%), sodium pyruvate (2 mM), non-essential amino acids (1%), penicillin/streptomycin antibiotics (0.2%), and β-mercaptoethanol (0.1%). Cultures were enriched for macrophages by overnight adherence. All cells were cultured at 37°C and 5% CO_2.

Light and laser-scanning-confocal microscopy

An aliquot of cell suspension equal to $5x10^4$ to $1x10^5$ cells was taken for cytospin analysis. The cytospin filter was primed with 100 µl PBS (300 rpm, 1 min) before addition of 200 µl cell suspension (300 rpm, 5 min). After an overnight drying step, cells were fixed in methanol for 30 min at -20°C and dried for 2 h. Cells were stained with undiluted May-Grünwald for 5 min (granular stain), washed in PBS, and stained for 20 min in 20x diluted Giemsa (nuclear stain). Cells received a final wash with bi-distilled water and were left to dry overnight. At least 200 cells were counted per treatment with a standard light microscope.

Live cells were stained with fluorescent markers for confocal microscopy at the time points specified in culture medium without amines and serum at 37°C for 30 min. Nuclear DNA was stained with Hoechst (1 µM), cellular cytoplasm with CellTracker™Red or CellTracker™Blue (10 µM) and neutral LDs with Bodipy®493/503 (8 µg/ml; Molecular Probes). Cells were washed three times in warm endotoxin-free PBS to remove unbound probe and fixed consecutively for 15 min in 2% then 4% paraformaldehyde. Macrophages were classified as enlarged vacuole-positive (V+) when their cell size was ≥24 µm and multiple large vacuoles were present. Fluorescently labelled cells were viewed on a Leica TCS SP5 AOBS inverted confocal microscope with a 63x HCX PL Apo 1.4 oil objective and stacked images taken at 0.42 µm slices with a spectral photomultipliers DFC320 colour camera (36-bit, 7 megapixels, non-confocal). Training and technical support was provided by the Bio Imaging Core facility of the Flemish Institute of Biotechnology (Ghent).

Quantification of intracellular cholesterol content

Macrophage intracellular cholesterol was quantified using the Calbiochem® cholesterol/cholesteryl ester quantitation kit (Merck Millipore, Cat. No.428901). Cell pellets ($1x10^6$ cells) were freeze-thawed five times in liquid nitrogen, homogenised with pestle in 200 µl chloroform:isopropanol:NP40 (7:11:0.1, v/v/v) and centrifuged for 10 min at 14,000 rpm. The organic lower phase was transferred to a clean microcentrifuge tube and air-dried at 50°C. To remove any residual chloroform, samples were further vacuum-dried for 30 min at 45°C. The dried lipids were dissolved in 200 µl cholesterol reaction buffer at 40°C for two cycles of heating (10 min) and vortexing with a final vortex of 5 min. All extracted samples and standards were added to a volume of 50 µl in a black 96-well plate followed by 50 µl of reaction mix 1 (with cholesterol esterase) or 2 (without cholesterol esterase) for determination of total cholesterol and free cholesterol, respectively. The assay plate was incubated at 37°C for 60 min; then fluorometrically measured on a FLUOstar OMEGA microplate reader (~535/590 nm). Cholesterol standards were plotted against relative fluorescence units and the concentration of total, free and esterified cholesterol (free subtracted from total) calculated as $µg/10^6$ cells.

Statistical analyses

The number of mice used for experiments comprised a minimum of five mice per treatment. Data were obtained from at least three independent experiments or 500 cells from no less than five separate microscopy images. The distribution of all data was determined by a Shapiro-Wilk (*W*) normality test. Nonparametric Mann-Whitney *U* or Kruskal-Wallis one-way analysis of variance tests (*H*; with Dunn's ranked sum multiple comparisons) were used to assess the proportion of foam cells in PEC cytospins and cellular cholesterol content (dependent variables) for each treatment or cholesterol fraction (categorical variables). Generalised linear model analyses (GLM: Poisson distribution with sequential Sidak pairwise comparisons) were used to assess counts of the number of cellular vacuoles, LDs, and bacilli (dependent variables) for each treatment or MOI at specified time points (predictors). Image processing and quantification of cellular markers for confocal microscopy were conducted with Volocity 3D Image Analysis Software (PerkinElmer Inc.). All other statistical analyses were performed with IBM SPSS Statistics 23 (IBM, Chicago IL, USA) and GraphPad Prism 5 (GraphPad Software, Inc.). Results were presented as mean ± standard error of the mean (SEM) and were considered significant at $P \leq 0.05$.

Results

Mycolic acids of the methoxy oxygenation class promote the formation of multi-vacuolar foam cells

To assess the influence of MA structure on the induction of multi-vacuolar giant foam cells, mice were i.p. injected with 25 µg of various MAs (alpha, methoxy or keto) (Fig. 1) or control compounds (PBS or liposome carrier without synthetic MA). PECs were harvested two days after treatment. Macrophages were examined by cytospin analysis and laser-scanning-confocal microscopy. PEC from mice treated with PBS, liposome carrier without synthetic MA (Lipo) and αMA-containing liposomes contained <10% vacuolar foam cells (Fig. 2A-B). In contrast, PEC from mice treated with liposomes containing kMA or mMA showed ~15% and 27-30% vacuolar foam cells, respectively. GLM analysis showed a clear difference among the treatments in their ability to induce vacuoles. mMA clearly effected vacuole formation with significantly more enlarged vacuole-positive (V+) cells (25-35%) as compared to kMA (5-

10%) and other treatments (<5%) (Fig. 2C-D). In addition, the proportion of enlarged V+ cells from the mMA cell population remained significantly elevated over time when kept in culture. At the 48 h time point, the macrophages from mMA treatment remained enlarged, while all other treatments resulted in macrophages returning to normal size (<5% enlarged V+ cells) (Fig. 2C). MGCs were seen mainly among the enlarged V+ cells induced by mMA (Fig. 2E).

Mycolic acids of the keto oxygenation class induce foam cells rich in cholesterol-laden lipid droplets

A clear difference was observed among treatments in their ability to induce LD accumulation (Fig. 3). kMA significantly induced LDs, up to 3-fold higher in comparison to all other treatments (Fig. 3A). Clearly, kMA was the strongest inducer of intracellular lipids in peritoneal mouse macrophages at all time points assayed. In order to normalise for LDs involved in regular macrophage metabolic activity, the LD number in PBS-treated cells was selected as baseline value against which relative increases or decreases of LDs in other treatments were compared. From this relative analysis, kMA again emerged as the MA class that significantly and prominently induced an increment in LDs in the macrophages (Fig. 3B-C). To further substantiate and quantify the accumulation of LDs in kMA-treated macrophages, the levels of intracellular active cholesterol and stored cholesteryl ester was determined in peritoneal macrophages isolated two days after oxygenated mMA or kMA treatment. Macrophages from the kMA treatment contained substantial intracellular esterified cholesterol, which also accounted for 77% of the total cholesterol content (Fig. 3D). Thus, the ratio of esterified-to-free cholesterol was distinctly elevated in the LD inducing kMA treatment and not in vacuole inducing mMA treated cells (Fig. 3D-E).

Mycolic acid induced lipid droplet accumulation in macrophages promotes BCG proliferation

In order to determine to what extent LD induction by kMA or vacuole induction by mMA may affect mycobacterial growth, peritoneal macrophages from mice treated with kMA or mMA were infected with BCG-dsRed and cultured for five days (Fig. 4A). Control groups again consisted of peritoneal macrophages isolated from mice injected with PBS (placebo) or the unoxygenated αMA. Infection of the

macrophages with BCG did not abrogate the accumulation of LDs in kMA-treated macrophages, nor induce as such an accumulation of LDs in placebo- or mMA-treated macrophages (Fig. 4B, upper panel). Strikingly, BCG replication was strongly enhanced in the kMA-treated macrophages (Fig. 4C), resulting in a near 3-fold increment in BCG numbers compared to the placebo-treated macrophages or macrophages treated with mMA (Fig. 4B, lower panel; and 4D). Macrophages from mice treated with a natural mixture of MA made up of αMA (~53%), kMA (~9%) and mMA (~38%) showed an intermediate induction of LDs as well as BCG replication (Fig. 4B), indicating that the presence of either mMA and/or αMA does not inhibit the LD-inducing and BCG proliferative biological function of kMA.

Assessment of mycobacterial growth in LD-accumulating macrophages from LXR-deficient mice

In order to determine whether foamy macrophages brought about by non-tuberculous means would also display elevated intracellular mycobacterial growth similar to kMA-treated macrophages, we investigated this parameter in peritoneal macrophages from LXR-deficient KO mice. Macrophages deficient in LXR contained abundant LDs sustained over time (Fig. 5A). This was accompanied with intracellular accumulation of esterified-to-free cholesterol at a ratio of ~8:1 in KO mice (Fig. 5B). Strikingly, these LD-accumulating macrophages, elicited by a deficiency in LXR activity, also showed a significantly increased mycobacterial growth as compared to macrophages from WT mice (Fig. 5C).

Discussion

The hallmark response to Mtb infection is the formation of granulomas that, in spite of being crucial to host protection, are exploited by mycobacteria for survival and persistence (43). Granulomas contain distinct macrophage populations of which foam cells loaded with neutral lipids and giant cells containing abundant vacuoles are characteristic (44). It was shown previously that natural, purified Mtb MA induces cellular features similar to those observed in granuloma cell populations (25). However, as MAs are heterogeneous, we determined in this study to what extent examples of individual MA classes sustain the foamy and/or vacuolar giant cellular traits in macrophages. The clear difference reported here between

mMA and kMA treatment in murine macrophages – a distinct induction by mMA of vacuoles without LDs and an upregulation of LDs without vacuoles by kMA – indicates the occurrence of independent triggers for giant versus foamy cell phenotypes during Mtb infection. The pathophysiological significance of these independent macrophage responses possibly reflects a strategy by Mtb to persist inside the key immune effector cell responsible for its elimination (45-47). In nature, the inflammatory neutral αMA class makes up approximately 50% of all MAs whereas the ratio of pro-inflammatory mMA to kMA classes in the Mtb bacillus cell wall is variable and may be tuned to complement growth and persistence (13, 17, 18). Korf *et al.* (25) previously showed that macrophages from mice treated with the natural MA mixture (similar to the MA mix used in this study) containing approximately 32-40% methoxy mycolates, accumulated large intracellular vacuoles like those reported by us here after treatment with pure (100%) mMA. Our results furthermore showed that the macrophages harvested from mice after natural MA mix treatment, which contains 7-15% keto mycolates, significantly accumulated intracellular LDs and allowed for mycobacterial growth, comparable to the macrophages from the pure (100%) kMA treatment group, but reduced by about half. One could therefore anticipate that the changes brought about by regulation of the MA class composition by Mtb will not be extreme.

LDs are widespread cell organelles dedicated to the storage of neutral lipids like cholesteryl esters (48). Numerous studies have reported on the close association of this distinctive lipid organelle with Mtb pathogenesis (28, 46, 49-52). The dynamic interaction of the LD with the Mtb-containing vacuole was recorded in an *in vitro* granuloma model by Peyron and team (28). Electron microscopy analyses of foam cells showed that phagosomes containing bacilli migrated towards LDs and eventually engulfed them. D'Avila *et al.* (53) observed in a murine model of TB using the vaccine strain BCG, a dose-response in LD formation over time. Close associations between LDs and phagosomes were recorded in BCG-infected treatments, with significant LD induction observed after 24 hours that remained elevated for about two weeks after infection. Cytoskeleton arrangement and phosphatidylinositol-3-kinase, an enzyme involved in cellular regulation of proliferation, trafficking and metabolism (54), were identified to play

key roles in the LD recruitment to bacilli-enclosed phagosomes (55). It is thus clear that pathogenic mycobacteria regulate biogenesis or accumulation of host cell lipids into LD-confined organelles, which may be further manipulated to intimately associate with the phagosomes enclosing the bacilli. An important question is the pathophysiological relevance of this association. Research suggests that the LD-phagosome interaction serves a dual purpose: at one end to benefit the microorganism and at the other to aid the host cell in microbe elimination (28, 32, 56). LDs may serve as a nutrient source to the bacillus through direct assimilation of host cell lipids (28) or as nutrient reservoir during latency (32). In contrast, host cells employ LDs to disseminate important anti-bacterial factors as was recorded in an *in vitro* study of latex bead phagosomes and pathogenic mycobacteria (56). Phagosomes infected with Mtb and exposed to distinct lipids (i.e. arachidonate, ceramide and sphingomyelin) induced actin assembly in macrophages, a process involved in microtubule organisation and LD trafficking (55). Lipid exposure also effected phagolysosomal fusion and decreased phagosome pH, events indicative of phagosome maturation and engagement of bactericidal machinery (56). It was noted that the kMA induced LD accumulation in macrophages tended to rapidly return to normal after removing the kMA stimulation, while the mMA induced vacuolation of the macrophage was maintained after removal of mMA. Enlarged intracellular vacuoles, like those induced after treatment with mMA, represent structures formed by invagination of the external cell membrane phospholipid bilayer into the cytosol (57). These double-layered vacuoles form stable structures that essentially provide a compartment for upholding the bacterium. LDs are phospholipid monolayer organelles critically involved in cellular lipid metabolism (58). As dynamic structures mediating lipid exchange or consumption, removal of the LD-inducing stimulus can be expected to coincide with rapid turnover and/or catabolism of the LDs by cellular machinery.

As indicated above, we confirmed that αMA is functionally neutral and showed that the oxygenated MAs effected pronounced changes with remarkable segregation of foam cell features: mMA induced enlarged multi-vacuolar cells whereas kMA stimulated cells to accumulate LDs with most of its cholesterol converted to the cholesteryl ester storage form. We next verified the relevance of these responses to

intracellular growth of mycobacteria. Using kMA-induced foamy cells and mMA-induced giant cells, we infected these macrophages *ex vivo* with BCG-dsRed and measured replication of the bacilli over time. Our results showed that intracellular growth was promoted in kMA-induced foamy macrophages, but not in mMA-induced giant cells. Macrophages classically convert into foam cells through a dysregulation in the balance between influx and efflux of cholesterol. Cholesterol is transported to peripheral macrophages in LDL that are taken up by the cell through the LDL receptor, or in the oxidized form, through scavenger receptors SRA and CD36. Cholesterol efflux is mediated by the transporters ABCA1 and ABCG1 that load the cholesterol on HDL for transfer to the liver, a mechanism known as reverse cholesterol transport. These processes are regulated by the lipid sensing nuclear receptors LXR and PPARγ. A direct role for LXR in mycobacterial foam cell formation has not been reported. However, mice deficient in LXR show spontaneous foam cell formation (59). LXR-deficient macrophages may be considered a cell model of the late stage of Mtb infection, where the macrophage has been modified to shut off its cholesterol export without limiting cholesterol import, aiming at providing a rich sterol nutrition source for mycobacterial growth and replication. We therefore investigated whether foam cells generated through a non-infectious condition, namely a deficiency in LXR activity, would also facilitate growth and proliferation of BCG bacilli. Similar to macrophages from mice treated with kMA, LXR-deficient macrophages accumulated cholesteryl ester-rich LDs and were facilitative towards mycobacterial growth. LXR-deficient macrophages contained more than double the amount of cholesterol compared to what could be induced with kMA and facilitated proliferation to almost double the number of BCG mycobacteria per 100 cells after 96 hours. These results suggest that LXR may indirectly function as a negative regulator of mycobacterial foam cell formation and mycobacterial growth. Although speculative, this proposition is in line with a previous report showing that LXR-activity suppresses the outgrowth of Mtb bacilli in a mouse model of pulmonary Mtb infection (60).

Our study addressed the individual contribution that examples of each of the three main classes of MAs from Mtb makes towards the induction of foam cells and multi-vacuolar giant cells as well as towards the

facilitation of intracellular mycobacterial proliferation. All three features are important elements of the manifestation of TB in human lungs and were elicited to varying degrees by the individual MA classes studied. Thus, we showed here that it is kMA that induces mainly cholesterol ester accumulation within intracellular LDs and facilitates mycobacterial BCG proliferation. In contrast, mMA was found to induce vacuole formation, characteristic of giant cells found in Mtb lung granulomas, with however no change in cholesteryl ester content or an improved ability to sustain and facilitate mycobacterial growth. Finally, αMA treatment exerted a negligible effect on all three parameters. These findings suggest separate important roles for keto and methoxy oxygenated MA classes in manipulating the host macrophage response during the establishment of TB. This new insight may assist in deciphering and targeting the Achilles' heel of the tubercle bacillus according to an approach recently reviewed by Nataraj *et al*. (61), relying on the most recent understanding of how MA is synthesised and differentiated into classes by Mtb. Cyclopropanation provides the minimum functionalisation associated with MA virulence (17). Dubnau *et al*. (18) provided evidence that cyclopropanation or functionalisation of the distal group of the meromycolic chain represents the first step of a common pathway responsible for generating methoxy and keto mycolates. Differential regulation of this single mechanism can thus allow mycobacteria to manipulate MA class composition of alpha, methoxy and keto mycolates during growth progression. Evidence for this was provided by Yuan *et al*. (19), who showed that keto mycolates are more abundant during the early stage of mycobacterial infection, but gives way to methoxy mycolates that become more abundant in the later phase of infection. Our results imply that much may be accomplished by attempting to control the switch between methoxy and keto mycolates as a principle of drug treatment to combat TB. One argument for this was provided by Slama *et al*. (62) who showed that mMA was much more abundant in the virulent Mtb H37Rv strain than in the attenuated Mtb H37Ra strain. This has to be understood in the wider context that other differences between the H37Rv and H37Ra strains were also identified, but the researchers then achieved better resolution of the evidence (62): A recombinant Mtb H37Rv was generated with a single gene KO of a protein involved in the late stage of MA biosynthesis, namely HadC. HadC is a dehydratase that is not catalytically active, but holds the longer form of the

elongating merochain of MA in a complex with HadB, which catalyses dehydration of a β-hydroxyacyl in the merochain to an enoyl. The *hadC* KO Mtb H37Rv showed a reduction in the abundance of mMA similar to that found in Mtb H37Ra (62). It accordingly also had lower virulence, approximating that of Mtb H37Ra, lost its cording and biofilming ability and its envelope integrity, thus making it more susceptible to the hydrophobic drug rifampicin. It should be noted that these biological effects could not only be ascribed to the lowering of the abundance of mMA, because the *hadC* KO Mtb H37Rv also had a larger degree of unsaturation in the merochain and could not produce the small amount of extra-long chain MAs of all three classes that are present in the WT Mtb H37Rv.

Whereas the group of Slama (62) demonstrated the advantage of being able to reduce the abundance of mMA in Mtb, our results could imply that even more may be achieved by interfering with kMA production in Mtb. However, Dubnau *et al*. (18) managed to create a *hma*- KO mutant Mtb H37Rv that produced no oxygenated MA at all. The mutant Mtb also showed severe loss of virulence, but was still able to grow and multiply in a monocytic cell line or in lungs and spleen of infected mice. Thus, kMA seems not to be essential for survival of Mtb and is hence not a prime target for the conceptualisation of a new anti-TB drug; although we have demonstrated here how kMA allows the mycobacterium to thrive, but not survive, in the target host cell.

Acknowledgements/grant support: This work was supported by the National Research Foundation (South Africa), Fund for Scientific Research (FWO, Belgium) and TBVAC2020 consortium from the EU H2020 initiative to support the joint PhD research programme of Ilke Vermeulen at Ghent University and the University of Pretoria. The authors thank Dr Erica Houthuys (Inflammation Research Center, Ghent) and Prof. Ben Appelmelk (VU University Medical Centre, Amsterdam) for provision of the BCG-dsRed, the Bio Imaging Core facility of the Flemish Institute of Biotechnology (Ghent) for microscopy training, Dr Marnik Vuylsteke (Gnomixx, Ghent) for statistical analysis guidance and Dr Jan-Åke Gustafsson (Karolinska Institute, Sweden) for the LXR-KO mice.

Conflict of interest: The authors declare no conflict of interest regarding this manuscript.

Author contributions: IV conducted the experimental work, analysed the results, compiled the figures and wrote the complete first draft of the manuscript. JG and JV conceptualised the research. MB oversaw the MA synthesis and JAD provided the synthetic MAs. MS provided constructive critiques.

References

1. WHO. 2015. Global Tuberculosis Report. 20th ed. World Health Organization, Geneva. pp 204.

2. Pieters, J. 2008. *Mycobacterium tuberculosis* and the macrophage: maintaining a balance. *Cell Host Microbe* **3**: 399-407.

3. Jamwal, S. V., P. Mehrotra, A. Singh, Z. Siddiqui, A. Basu and K. V. Rao. 2016. Mycobacterial escape from macrophage phagosomes to the cytoplasm represents an alternate adaptation mechanism. *Sci. Rep.* **6**: 1-9.

4. Banerjee, S. K., M. Kumar, R. Alokam, A. K. Sharma, A. Chatterjee, R. Kumar, S. K. Sahu, K. Jana, R. Singh, P. Yogeeswari, D. Sriram, J. Basu and M. Kundu. 2016. Targeting multiple response regulators of *Mycobacterium tuberculosis* augments the host immune response to infection. *Sci. Rep.* **6**: 25851; doi: 25810.21038/srep25851.

5. Blischak, J. D., L. Tailleux, A. Mitrano, L. B. Barreiro and Y. Gilad. 2015. Mycobacterial infection induces a specific human innate immune response. *Sci. Rep.* **5**: 16882; doi: 16810.11038/srep16882.

6. Tsai, M. C., S. Chakravarty, G. Zhu, J. Xu, K. Tanaka, C. Koch, J. Tufariello, J. Flynn and J. Chan. 2006. Characterization of the tuberculous granuloma in murine and human lungs: cellular composition and relative tissue oxygen tension. *Cell. Microbiol.* **8**: 218-232.

7. Ramakrishnan, L. 2012. Revisiting the role of the granuloma in tuberculosis. *Nat. Rev. Immunol.* **12**: 352-366.

8. Yang, M., R. Lu, K. E. Guja, M. F. Wipperman, J. R. St Clair, A. C. Bonds, M. Garcia-Diaz and N. S. Sampson. 2015. Unraveling cholesterol catabolism in: ChsE4-ChsE5 alphabeta Acyl-CoA Dehydrogenase Initiates beta-Oxidation of 3-Oxo-cholest-4-en-26-oyl CoA. *ACS Infect. Dis.* **1**: 110-125.

9. Lee, W., B. C. VanderVen, R. J. Fahey and D. G. Russell. 2013. Intracellular *Mycobacterium tuberculosis* exploits host-derived fatty acids to limit metabolic stress. *J. Biol. Chem.* **288**: 6788-6800.

10. Griffin, J. E., A. K. Pandey, S. A. Gilmore, V. Mizrahi, J. D. McKinney, C. R. Bertozzi and C. M. Sassetti. 2012. Cholesterol catabolism by *Mycobacterium tuberculosis* requires transcriptional and metabolic adaptations. *Chem. Biol.* **19**: 218-227.

11. Jankute, M., J. A. Cox, J. Harrison and G. S. Besra. 2015. Assembly of the mycobacterial cell wall. *Annu. Rev. Microbiol.* **69**: 405-423.

12. Riley, L. W. 2006. Of mice, men and elephants: *Mycobacterium tuberculosis* cell envelope lipids and pathogenesis. *J. Clin. Invest.* **116**: 1475-1478.

13. Verschoor, J. A., M. S. Baird and J. Grooten. 2012. Towards understanding the functional diversity of cell wall mycolic acids of *Mycobacterium tuberculosis*. *Prog. Lipid Res.* **51**: 325-339.

14. Watanabe, M., Y. Aoyagi, M. Ridell and D. E. Minniken. 2001. Separation and characterization of individual mycolic acids in representative mycobacteria. *Microbiology* **147**: 1825-1837.

15. Watanabe, M., Y. Aoyagi, H. Mitome, T. Fujita, H. Naoki, M. Ridell and D. E. Minniken. 2002. Location of functional groups in mycobacterial meromycolate chains; the recognition of new structural principles in mycolic acids. *Microbiology* **148**: 1881-1902.

16. Ndlandla, F. L., V. Ejoh, A. C. Stoltz, B. Naicker, A. D. Cromarty, S. van Wyngaardt, M. Khati, L. S. Rotherham, Y. Lemmer, J. Niebuhr, C. R. Baumeister, J. R. Al-Dulayymi, H. Swai, M. S. Baird and J. A. Verschoor. 2016. Standardization of natural mycolic acid antigen composition and production for use in biomarker antibody detection to diagnose active tuberculosis. *J. Immunol. Methods* **435**: 50-59.

17. Glickman, M. S., J. S. Cox and W. R. Jacobs, Jr. 2000. A novel mycolic acid cyclopropane synthetase is required for cording, persistence and virulence of *Mycobacterium tuberculosis*. *Mol. Cell* **5**: 717-727.

18. Dubnau, E., J. Chan, C. Raynaud, V. P. Mohan, M.-A. Laneelle, K. Yu, A. Quemard, S. Smith and M. Daffe. 2000. Oxygenated mycolic acids are necessary for virulence of *Mycobacterium tuberculosis* in mice. *Mol. Microbiol.* **36**: 630-637.

19. Yuan, Y., Y. Zhu, D. D. Crane and C. E. Barry, 3rd. 1998. The effect of oxygenated mycolic acid composition on cell wall function and macrophage growth in *Mycobacterium tuberculosis*. *Mol. Microbiol.* **29**: 1448-1458.

20. Ishikawa, E., T. Ishikawa, Y. S. Morita, K. Toyonaga, H. Yamada, O. Takeuchi, T. Kinoshita, S. Akira, Y. Yoshikai and S. Yamasaki. 2009. Direct recognition of the mycobacterial glycolipid, trehalose dimycolate, by C-type lectin Mincle. *J. Exp. Med.* **206**: 2879-2888.

21. Moody, D. B., G. S. Besra, I. A. Wilson and S. A. Porcelli. 1999. Molecular basis of CD1-mediated presentation of lipid antigens. *Immunol. Rev.* **172**: 285-296.

22. Karakousis, P. C., W. R. Bishai and S. E. Dorman. 2004. *Mycobacterium tuberculosis* cell envelope lipids and the host immune response. *Cell. Microbiol.* **6**: 105-116.

23. van der Meer-Janssen, Y. P., J. van Galen, J. J. Batenburg and J. B. Helms. 2010. Lipids in host-pathogen interactions: pathogens exploit the complexity of the host cell lipidome. *Prog. Lipid Res.* **49**: 1-26.

24. Cole, S. T., R. Brosch, J. Parkhill, T. Garnier, C. Churcher, D. Harris, S. V. Gordon, K. Eigleimer, S. Gas, C. E. Barry, F. Tekaia, K. Badcock, D. Basham, D. A. Brown, T. Chillingworth, R. Connor, R. Davies, K. Devlin, T. Feltwell, S. Gentles, N. Hamlin, S. Holroyd, T. Hornsby, K. Jagels, A. Krogh, J. McLean, S. Moule, L. Murphy, K. Oliver, J. Osborne, M. A. Qual, M.-A. Rajandream, J. Rogers, S. Rutter, K. Seeger, J. Skelton, S. Squares, J. E. Sulston, K. Taylor, S. Whitehead and B. G. Barrell. 1998. Deciphering the biology of *Mycobacterium tuberculosis* from the complete genome sequence. *Nature* **393**: 537-544.

25. Korf, J., A. Stoltz, J. Verschoor, P. De Baetselier and J. Grooten. 2005. The *Mycobacterium tuberculosis* cell wall component mycolic acid elicits pathogen-associated host innate immune responses. *Eur. J. Immunol.* **35**: 890-900.

26. Korf, J. E., G. Pynaert, K. Tournoy, T. Boonefaes, A. Van Oosterhout, D. Ginneberge, A. Haegeman, J. A. Verschoor, P. De Baetselier and J. Grooten. 2006. Macrophage reprogramming by mycolic acid promotes a tolerogenic response in experimental asthma. *Am. J. Respir. Crit. Care Med.* **174**: 152-160.

27. Russell, D. G., P. J. Cardona, M. J. Kim, S. Allain and F. Altare. 2009. Foamy macrophages and the progression of the human tuberculosis granuloma. *Nat. Immunol.* **10**: 943-948.

28. Peyron, P., J. Vaubourgeix, Y. Poquet, F. Levillain, C. Botanch, F. Bardou, M. Daffe, J. F. Emile, B. Marchou, P. J. Cardona, C. de Chastellier and F. Altare. 2008. Foamy macrophages from tuberculous patients' granulomas constitute a nutrient-rich reservoir for *M. tuberculosis* persistence. *PLoS Pathog.* **4**: e1000204. doi:1000210.1001371/journal.ppat.1000204.

29. Caceres, N., G. Tapia, I. Ojanguren, F. Altare, O. Gil, S. Pinto, C. Vilaplana and P. J. Cardona. 2009. Evolution of foamy macrophages in the pulmonary granulomas of experimental tuberculosis models. *Tuberculosis* **89**: 175-182.

30. Maxfield, F. R. and G. van Meer. 2010. Cholesterol, the central lipid of mammalian cells. *Curr. Opin. Cell Biol.* **22**: 422-429.

31. Guo, Y., K. R. Cordes, R. V. Farese, Jr. and T. C. Walther. 2009. Lipid droplets at a glance. *J. Cell Sci.* **122**: 749-752.

32. Pandey, A. K. and C. M. Sassetti. 2008. Mycobacterial persistence requires the utilization of host cholesterol. *Proc. Natl. Acad. Sci. U. S. A.* **105**: 4376-4380.

33. Brzostek, A., J. Pawelczyk, A. Rumijowska-Galewicz, B. Dziadek and J. Dziadek. 2009. *Mycobacterium tuberculosis* is able to accumulate and utilize cholesterol. *J. Bacteriol.* **191**: 6584-6591.

34. Jakobsson, T., E. Treuter, J. A. Gustafsson and K. R. Steffensen. 2012. Liver X receptor biology and pharmacology: new pathways, challenges and opportunities. *Trends Pharmacol. Sci.* **33**: 394-404.

35. A-Gonzalez, N. and A. Castrillo. 2011. Liver X receptors as regulators of macrophage inflammatory and metabolic pathways. *Biochim. Biophys. Acta* **1812**: 982-994.

36. Al Dulayymi, J. a. R., M. S. Baird and E. Roberts. 2005. The synthesis of a single enantiomer of a major α-mycolic acid of *M. tuberculosis*. *Tetrahedron* **61**: 11939-11951.

37. Al Dulayymi, J. a. R., M. S. Baird, E. Roberts, M. Deysel and J. Verschoor. 2007. The first syntheses of single enantiomers of the major methoxymycolic acid of *Mycobacterium tuberculosis*. *Tetrahedron* **63**: 2571-2592.

38. Koza, G. and M. S. Baird. 2007. The first synthesis of single enantiomers of ketomycolic acids. *Tetrahedron Lett.* **48**: 2165-2169.

39. Alberti, S., G. Schuster, P. Parini, B. Feltkamp, U. Diczfalusy, M. Rudling, B. Angelin, I. Björkhem, S. Pettersson and J.-Å. Gustafsson. 2001. Hepatic cholesterol metabolism and resistance to dietary cholesterol in LXRbeta-deficient mice. *J. Clin. Invest.* **107**: 565-573.

40. Abadie, V., E. Badell, P. Douillard, D. Ensergueix, P. J. Leenen, M. Tanguy, L. Fiette, S. Saeland, B. Gicquel and N. Winter. 2005. Neutrophils rapidly migrate via lymphatics after *Mycobacterium bovis* BCG intradermal vaccination and shuttle live bacilli to the draining lymph nodes. *Blood* **106**: 1843-1850.

41. Sani, M., E. N. Houben, J. Geurtsen, J. Pierson, K. de Punder, M. van Zon, B. Wever, S. R. Piersma, C. R. Jimenez, M. Daffe, B. J. Appelmelk, W. Bitter, N. van der Wel and P. J. Peters. 2010. Direct visualization by cryo-EM of the mycobacterial capsular layer: a labile structure containing ESX-1-secreted proteins. *PLoS Pathog.* **6**: e1000794.

42. Minnikin, D. E., J. H. Parlett, M. Magnusson, M. Ridell and A. Lind. 1984. Mycolic acid patterns of representatives of *Mycobacterium bovis* BCG. *J. Gen. Microbiol.* **130**: 2733-2736.

43. Davis, J. M. and L. Ramakrishnan. 2009. The role of the granuloma in expansion and dissemination of early tuberculous infection. *Cell* **136**: 37-49.

44. Puissegur, M. P., C. Botanch, J. L. Duteyrat, G. Delsol, C. Caratero and F. Altare. 2004. An i*n vitro* dual model of mycobacterial granulomas to investigate the molecular interactions between mycobacteria and human host cells. *Cell. Microbiol.* **6**: 423-433.

45. Venugopal, A., R. Bryk, S. Shi, K. Rhee, P. Rath, D. Schnappinger, S. Ehrt and C. Nathan. 2011. Virulence of *Mycobacterium tuberculosis* depends on lipoamide dehydrogenase, a member of three multienzyme complexes. *Cell Host Microbe* **9**: 21-31.

46. Singh, V., S. Jamwal, R. Jain, P. Verma, R. Gokhale and K. V. Rao. 2012. *Mycobacterium tuberculosis*-driven targeted recalibration of macrophage lipid homeostasis promotes the foamy phenotype. *Cell Host Microbe* **12**: 669-681.

47. Huang, Z., Q. Luo, Y. Guo, J. Chen, G. Xiong, Y. Peng, J. Ye and J. Li. 2015. *Mycobacterium tuberculosis*-induced polarization of human macrophage orchestrates the formation and development of tuberculous granulomas i*n vitro*. *PLoS One* **10**: e0129744. doi:0129710.0121371/journal.pone.0129744.

48. Krahmer, N., Y. Guo, R. V. Farese, Jr. and T. C. Walther. 2009. SnapShot: Lipid Droplets. *Cell* **139**: DOI 10.1016/j.cell.2009.1011.1023.

49. Lovewell, R. R., C. M. Sassetti and B. C. VanderVen. 2016. Chewing the fat: lipid metabolism and homeostasis during *M. tuberculosis* infection. *Curr. Opin. Microbiol.* **29**: 30-36.

50. Daniel, J., H. Maamar, C. Deb, T. D. Sirakova and P. E. Kolattukudy. 2011. *Mycobacterium tuberculosis* uses host triacylglycerol to accumulate lipid droplets and acquires a dormancy-like phenotype in lipid-loaded macrophages. *PLoS Pathog.* **7**: doi:10.1371/journal.ppat.1002093.

51. Kim, M. J., H. C. Wainwright, M. Locketz, L. G. Bekker, G. B. Walther, C. Dittrich, A. Visser, W. Wang, F. F. Hsu, U. Wiehart, L. Tsenova, G. Kaplan and D. G. Russell. 2010. Caseation of human tuberculosis granulomas correlates with elevated host lipid metabolism. *EMBO Mol. Med.* **2**: 258-274.

52. Deb, C., C.-M. Lee, V. M. Dubey, J. Daniel, B. Abomoelak, T. D. Sirakova, S. Pawar, L. Rogers and P. E. Kolattukudy. 2009. A novel *in vitro* multiple-stress dormancy model for *Mycobacterium tuberculosis* generates a lipid-loaded, drug-tolerant, dormant pathogen. *PLoS One* **6**: 1-15.

53. D'Avila, H., R. C. N. Melo, G. G. Parreira, E. Werneck-Barroso, H. C. Castro-Faria-Neto and P. T. Bozza. 2006. *Mycobacterium bovis* Bacillus Calmette-Guerin induces TLR2-mediated formation of lipid bodies: intracellular domains for eicosanoid synthesis *in vivo*. *J. Immunol.* **176**: 3087-3097.

54. Fruman, D. A. and C. Rommel. 2014. PI3K and cancer: lessons, challenges and opportunities. *Nat. Rev. Drug Discov.* **13**: 140-156.

55. Mattos, K. A., F. A. Lara, V. G. Oliveira, L. S. Rodrigues, H. D'Avila, R. C. Melo, P. P. Manso, E. N. Sarno, P. T. Bozza and M. C. Pessolani. 2011. Modulation of lipid droplets by *Mycobacterium leprae* in Schwann cells: a putative mechanism for host lipid acquisition and bacterial survival in phagosomes. *Cell. Microbiol.* **13**: 259-273.

56. Anes, E., M. P. Kuhnel, E. Bos, J. Moniz-Pereira, A. Habermann and G. Griffiths. 2003. Selected lipids activate phagosome actin assembly and maturation resulting in killing of pathogenic mycobacteria. *Nat. Cell Biol.* **5**: 793-802.

57. van Meer, G. 2011. Dynamic transbilayer lipid asymmetry. *Cold Spring Harb. Perspect. Biol.* **3**: 1-11.

58. Pol, A., S. P. Gross and R. G. Parton. 2014. Biogenesis of the multifunctional lipid droplet: lipids, proteins, and sites. *J. Cell Biol.* **204**: 635-646.

59. Schuster, G. U. 2002. Accumulation of foam cells in liver X receptor-deficient mice. *Circulation* **106**: 1147-1153.

60. Korf, H., S. Vander Beken, M. Romano, K. R. Steffensen, B. Stijlemans, J. A. Gustafsson, J. Grooten and K. Huygen. 2009. Liver X receptors contribute to the protective immune response against *Mycobacterium tuberculosis* in mice. *J. Clin. Invest.* **119**: 1626-1637.

61. Nataraj, V., C. Varela, A. Javid, A. Singh, G. S. Besra and A. Bhatt. 2015. Mycolic acids: deciphering and targeting the Achilles' heel of the tubercle bacillus. *Mol. Microbiol.* **98**: 7-16.

62. Slama, N., S. Jamet, W. Frigui, A. Pawlik, D. Bottai, F. Laval, P. Constant, A. Lemassu, K. Cam, M. Daffe, R. Brosch, N. Eynard and A. Quemard. 2016. The changes in mycolic acid structures caused by hadC mutation have a dramatic effect on the virulence of *Mycobacterium tuberculosis*. *Mol. Microbiol.* **99**: 794-807.

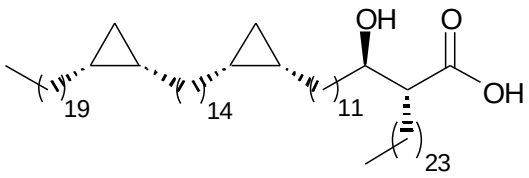

JR1080, **αMA** (19,14,11,23)

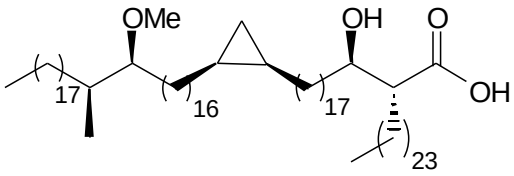

JR1046, **mMA** (17,16,17,23)

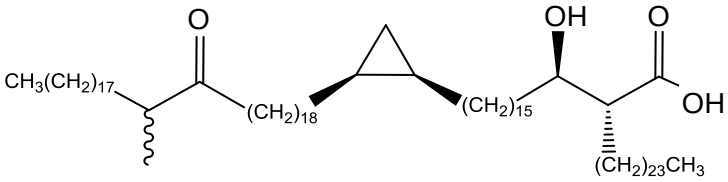

GK324, **kMA** (17,16,17,23)

Figure 1. Mycolic acid structures. The biochemical structures of the synthetic MAs are given for examples of the alpha (αMA; JR1080), methoxy (mMA; JR1046) and keto (kMA; GK324) classes containing *cis*-cyclopropanation. Numbers in brackets represent carbon chain lengths and wiggly line indicates a mixture of stereoisomers at that position.

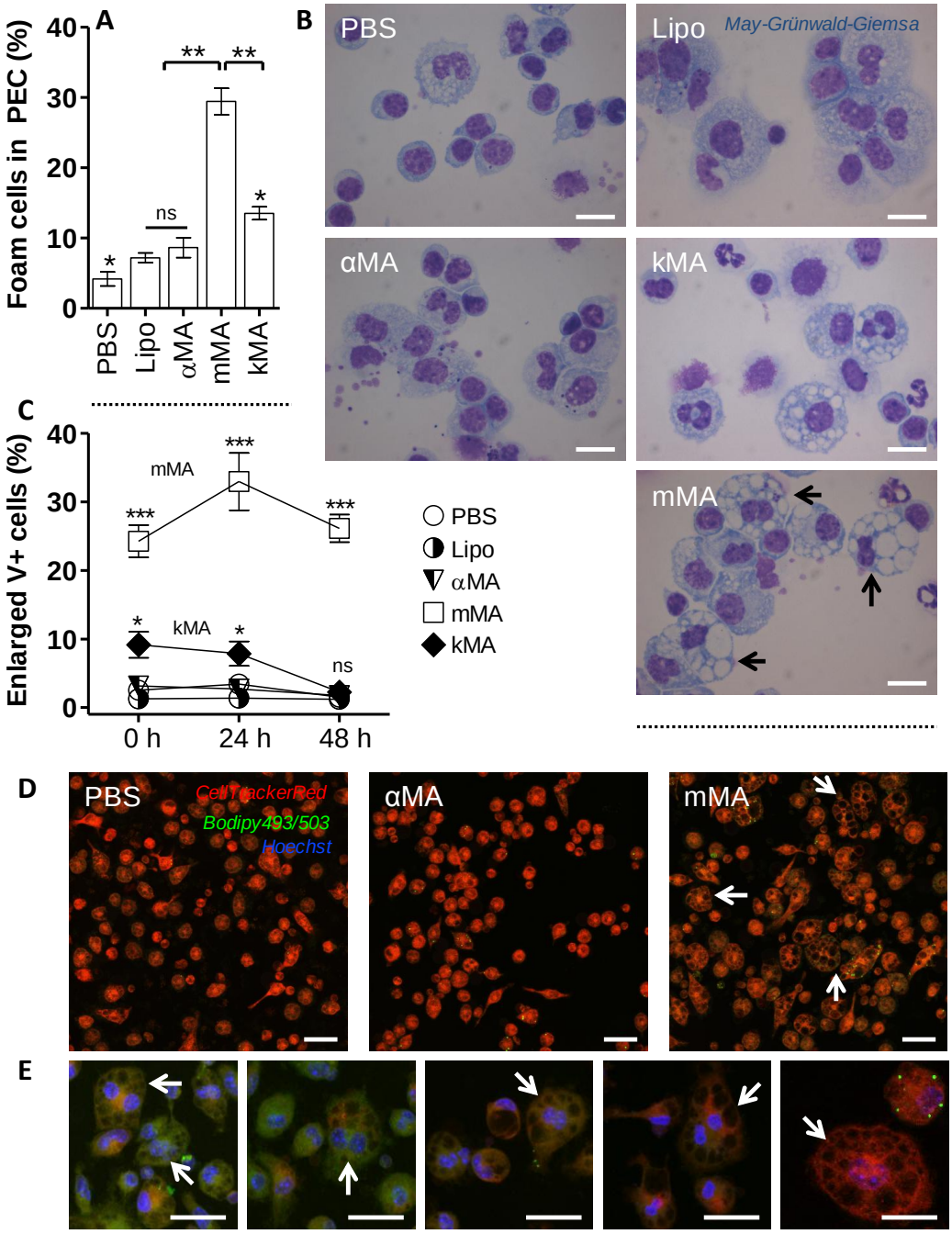

Figure 2. **Mycolic acids of the methoxy oxygenation class promote the formation of multi-vacuolar foam cells**. The proportion of vacuole-rich macrophages was determined by light microscope images of May-Grünwald-Giemsa stained cells on cytospins and by laser-scanning-confocal microscopy (mean ± SEM). (A) Percentage of foam cells in PEC fraction from the control (PBS and Lipo), αMA, mMA and kMA treatments. (Shapiro-Wilk: $W = 0.801$, $P < 0.01$; Kruskal-Wallis: $H = 12.100$, $P < 0.05$, $df = 4$, $n = 3$ independent experiments). (B) Light microscope images of cytospins showing vacuolar foam cells in PEC fraction. Images were taken at 100x oil magnification. Arrows indicate multinucleated giant cells (MGCs). Scale bar: 10 µm. (C) Induction of enlarged vacuole-positive (V+) cells is shown for control (PBS and Lipo) and the various MA-treated mouse peritoneal macrophages over time, as measured by laser scanning confocal microscopy (GLM: Wald Chi-Square = 753.924, $P < 0.001$, $df = 14$, $n = 5$ per time point). (D-E) Laser scanning confocal microscopy images showing enlarged V+ cells for PBS, αMA and mMA treatments. Arrows indicate MGCs. Stacked images, 63x oil objective. Scale bar: 20 µm. (E) Zoomed images from the mMA treatment in D.

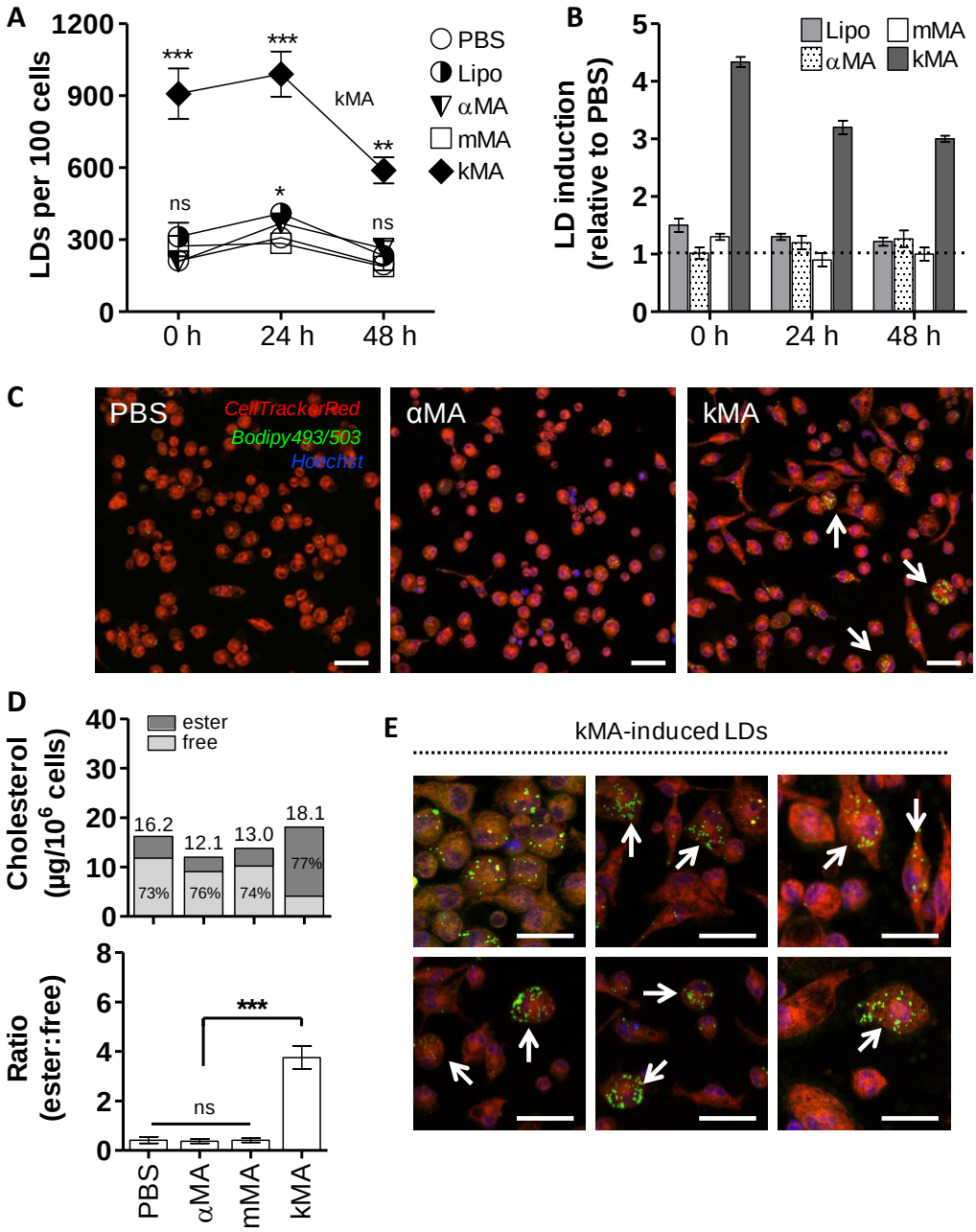

Figure 3. Mycolic acids of the keto oxygenation class induce foam cells rich in cholesterol-laden lipid droplets. The induction of LDs is shown for peritoneal macrophages from control (PBS and Lipo) and αMA, mMA and kMA-treated mice (mean ± SEM). (A) LD accumulation in murine macrophages harvested at specified time points following the control and various MA treatments (GLM: Wald Chi-Square = 353.662, $P < 0.001$, df =14, n = 5 per time point). (B) Relative induction of LDs over time as compared to PBS (broken line). (C) Laser-scanning-confocal microscopy images depicting variation in LD induction for PBS, αMA and kMA treatments. Arrows indicate LD filled cells. (D) Cellular cholesterol content of variously treated cells. Bars represent total cholesterol, subdivided in the amount of free and esterified cholesterol for each of the treatments (µg/10^6 cells). Upper panel, fraction percentages of free and esterified cholesterol are shown in the bars (n = 12 mice; Shapiro-Wilk: W = 0.813, $P < 0.05$; Kruskal-Wallis: H = 24.726, $P < 0.001$, df = 3). Lower panel, the ratio of esterified-to-free cholesterol is given for the various treatments (Kruskal-Wallis: H = 26.554, $P < 0.001$, df = 3). (E) kMA induced LDs in peritoneal macrophages as identified by the neutral lipid probe Bodipy®493/503. (C, E) Stacked images, 63x oil objective. Scale bar: 20 µm.

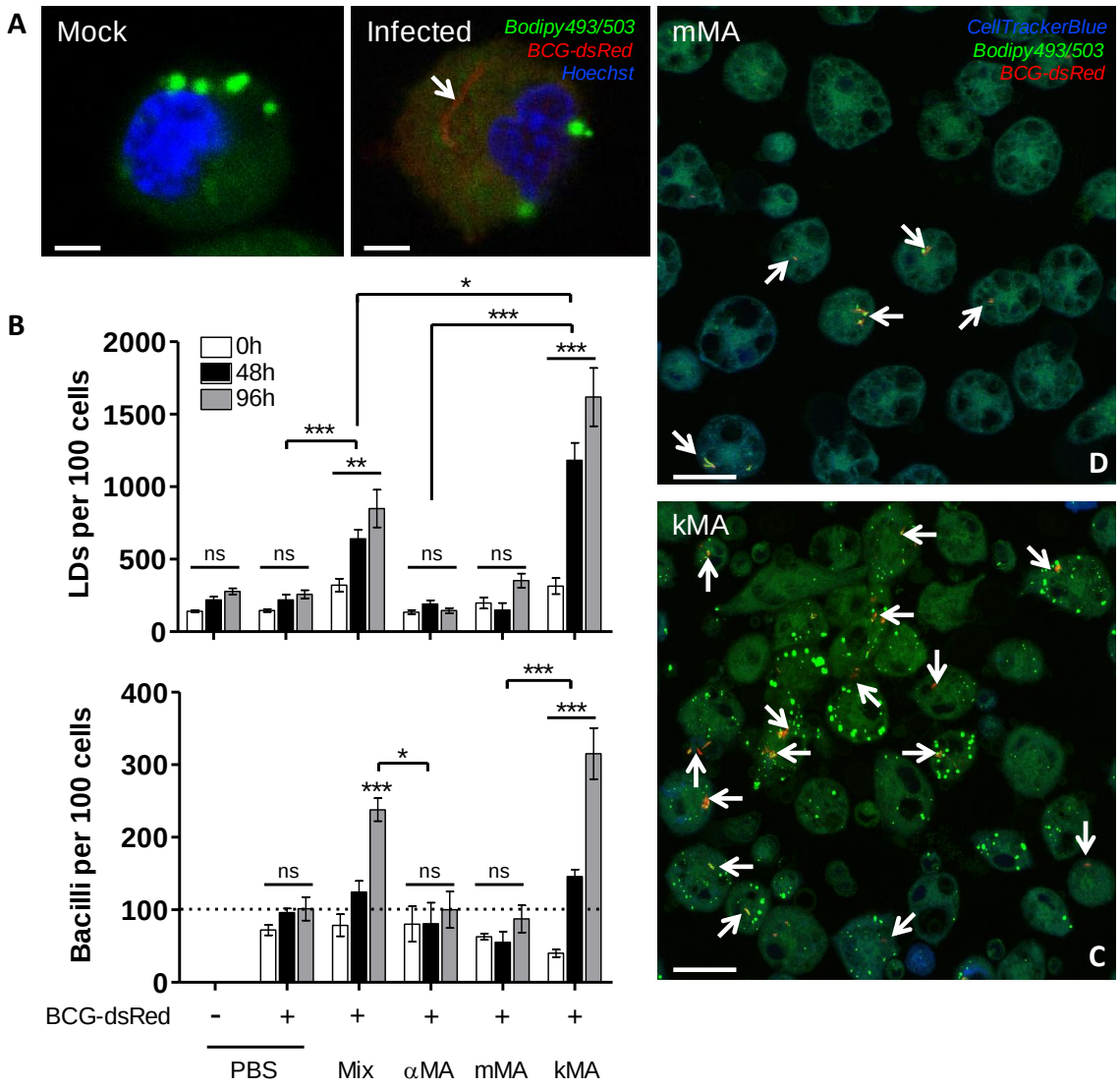

Figure 4. Mycolic acid induced lipid droplet accumulation in macrophages promotes BCG proliferation. Following *in vivo* treatment with MA, peritoneal macrophages were infected *ex vivo* with BCG-dsRed (MOI 1, broken line) and cultured until timed interval measurements were taken by laser-scanning-confocal microscopy (mean ± SEM). (A) Laser-scanning-confocal microscopy images (zoomed) showing macrophages from mock or BCG infections. The presence of a BCG-dsRed bacillus can be clearly distinguished. Scale bar: 2.5 µm. (B) Upper panel, LD accumulation in peritoneal macrophages over time (GLM: Wald Chi-Square = 636.496, $P < 0.001$, $df = 17$, $n = 5$ per time point). Lower panel, proliferation of BCG bacilli over time (GLM: Wald Chi-Square = 250.303, $P < 0.001$, $df = 17$, $n = 5$ per time point). On the X-axis, "Mix" denotes a natural purified MA extract consisting of ~53% αMA, ~38% mMA and ~9% kMA. (C-D) Laser-scanning-confocal microscopy images depicting a clear difference in the presence of BCG-dsRed bacilli in peritoneal macrophages from mice treated with either kMA or mMA. Stacked images, 63x oil objective. Scale bar: 20 µm. Arrows indicate BCG-dsRed bacilli.

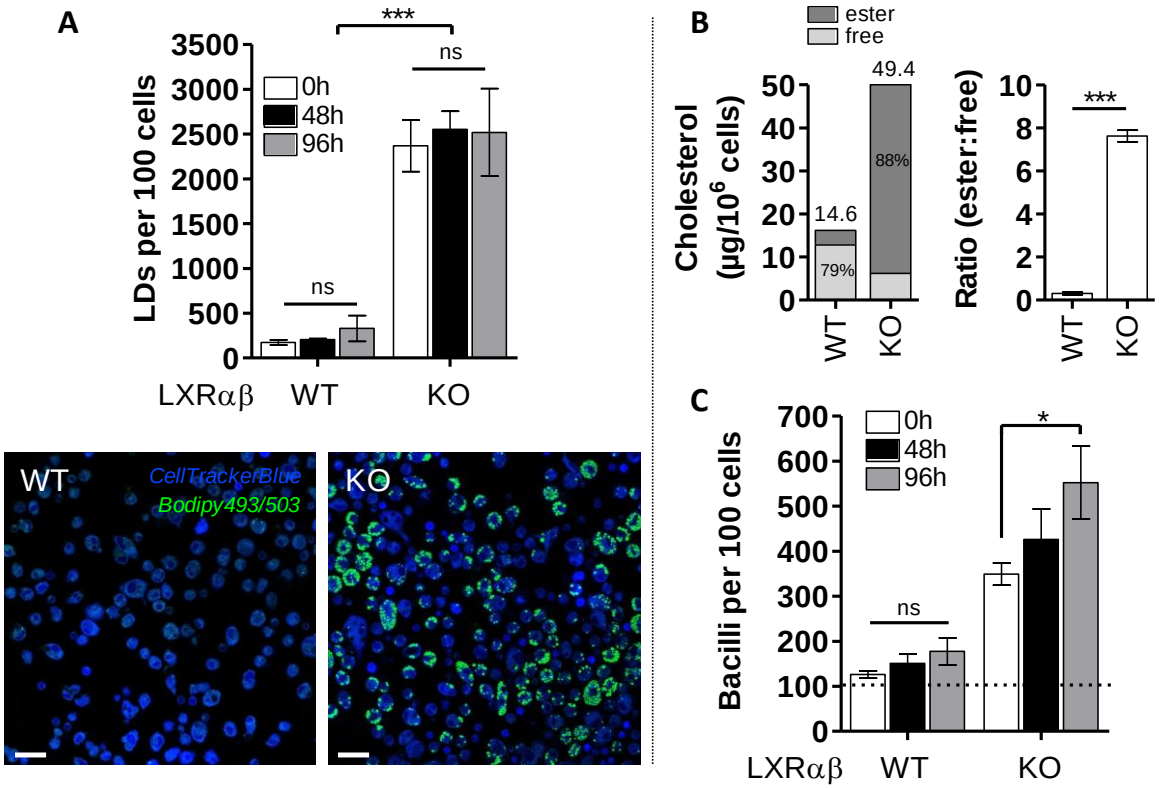

Figure 5. Mycobacterial growth in lipid droplet accumulating macrophages from LXR-deficient mice. (A) Macrophages from WT and LXR-deficient mice were cultured for five days and the intracellular LD prevalence analysed by laser-scanning-confocal microscopy. KO-cells contained ~10-fold more cellular LDs in comparison to WT-cells, though no significant change in the number of LDs per 100 cells was observed over time (GLM: Wald Chi-Square = 99.093, $P < 0.001$, $df = 5$, $n = 4$ per time point; sequential Sidak pairwise comparisons $P > 0.05$). Laser-scanning-confocal microscopy images depicting clear morphological differences in LD prevalence between WT and KO macrophages. Scale bar: 20 µm. (B) Cholesteryl esters accounted for 88% of total cholesterol in LXR-deficient cells (left panel) that also contained significantly elevated ratios of intracellular esterified-to-free cholesterol (right panel; Mann-Whitney: $U = 144.000$, $P < 0.001$, $df = 1$, $n = 12$ mice). (C) Macrophages from WT and KO mice were infected *ex vivo* for 6 h with BCG-dsRed (MOI 1, broken line) and cultured for five days. Mycobacterial growth was measured by laser-scanning-confocal microscopy at specified time points, and was significantly increased in LXR-deficient cells over time (GLM: Wald Chi-Square = 576.689, $P < 0.001$, $df = 17$; $n = 6$ per time point; sequential Sidak pairwise comparisons $P < 0.05$). Data represent mean ± SEM.